frontiers | Frontiers in Physics

ORIGINAL RESEARCH
published: 18 May 2022
doi: 10.3389/fphy.2022.909318

Lamb Wave Propagation Control Based on Modified GSL

Huagen Yang, Kan Feng, Rong Li and Jing Yan*

Faculty of Civil Engineering and Mechanics, Jiangsu University, Zhenjiang, China

As a new kind of elastic materials, elastic wave metasurface has great research significance in the field of elastic wave regulation. However, most of the researches on elastic wave metasurface are guided by traditional Generalized Snell's Law (GSL), and the effect of higher order diffraction waves caused by structural periodicity is not considered. Under the action of higher order diffraction wave, the incident wave will produce more complex transmission phenomenon when passing through the metasurface, and the angle of transmission does not conform to GSL in some cases. In order to verify whether the modified GSL theory considering the higher-order diffraction term is still applicable to the regulation of solid elastic waves, this paper designs a helical metasurface based on the elastic wave theory of plate-beam structure, which is composed of helical lines of different lengths, and uses this structure to explain the complex transmission phenomenon of elastic wave metasurface. Finally, the asymmetric transmission, modal separation and waveguide of Lamb waves in thin plates are realized by combining the theory with structural design, which proves that the structure has great application potential in ultrasonic detection and other fields.

Keywords: elastic wave metasurface, modified GSL theory, lamb wave, asymmetric propagation, mode separation, waveguide

OPEN ACCESS

Edited by:
Kaijun Yi,
Beijing Institute of Technology, China

Reviewed by:
Chen Shen,
Rowan University, United States
Yan-Feng Wang,
Tianjin University, China

****Correspondence:***
Kan Feng
fengkan@ujs.edu.cn

Specialty section:
This article was submitted to Physical Acoustics and Ultrasonics, a section of the journal Frontiers in Physics

Received: *31 March 2022*
Accepted: *29 April 2022*
Published: *18 May 2022*

Citation:
Yang H, Feng K, Li R and Yan J (2022) Lamb Wave Propagation Control Based on Modified GSL. Front. Phys. 10:909318. doi: 10.3389/fphy.2022.909318

1 INTRODUCTION

Elastic waves are a classical form of motion in engineering structures, and the mechanical vibrations of major equipment such as aerospace vehicles, underwater probes, and high-speed trains are essentially the superimposed effects of their internal elastic waves. With the depth of research, the regulation of elastic waves has gradually become the focus of attention, and the emergence of metasurface structures [1–3] in recent years is one of the means to effectively regulate elastic waves.

In 2011, Yu et al [4] introduced phase mutation at the interface through a periodic array of V-shaped antennas to reach the modulation of the phase of the incident light wave and further realize the anomalous reflection and transmission of the wave, and the reflection and transmission angles satisfy the so-called Generalized Snell's Law (GSL). The proposed GSL shows that it is possible to introduce the phase mutation through a two-dimensional interface, and thus a series of anomalous acoustic phenomena such as negative refraction and acoustic focusing can be realized more easily and conveniently. In 2013, Li et al [5] extended GSL from optics to acoustics and designed a spatially folded metasurface to discretize the phase gradient to achieve anomalous reflection and acoustic focusing. Since then, a large number of studies have emerged on the use of metasurfaces to modulate the phase of acoustic waves. In 2014, Xie et al [6] pointed out that due to the periodicity of the metasurface structure, higher-order diffraction occurs when the incident wave is larger than a certain critical angle, and the transmission angle no longer satisfies the GSL, and the higher-order diffraction term needs to be introduced to correct the law. However, after related studies, it is shown that the corrected law still cannot explain all the anomalies well. In 2019, the correction theory was further

supplemented by Fu et al [7], who pointed out that the higher-order diffraction waves in the metasurface exhibit alternating reflection and transmission, and the factor affecting whether the reflection or transmission occurs is the number of structural unit cells.

The study of acoustic wave metasurfaces has matured in the last decade. However, in the study of elastic wave metasurfaces, since elastic waves in solids have more degrees of freedom and more complicated wave equations, transverse waves and longitudinal waves, as well as various forms of waves formed by mutual coupling, are often accompanied by the mode conversion is obviously more complicated than the single longitudinal wave mode in air and liquid, which directly leads to the late start of research on elastic wave metasurfaces. It was not until 2016 that the concept of acoustic wave metasurfaces was further extended to elastic wave metasurfaces by Semperlotti et al [8], who designed a conical column metasurface structure. When a plate wave passes through this structure in a periodic arrangement, a weak local resonance effect occurs, which leads to mode conversion and thus to transmission manipulation of A_0 waves. In 2017, Liu et al [9] realized a bending wave vibration source phantom by constructing a sawtooth type structure. In 2020, Yuan et al [10] ingeniously designed a "fishbone" type semi-active metasurface, which could regulate the phase of transmitted waves by rotating the nuts, and in 2021, Yaw et al [11] introduced a coded negative capacitance circuit in the metasurface to achieve active modulation of longitudinal waves. During this period, there are still some researches on the use of metasurfaces to modulate elastic waves [12–29], mainly including the ingenious design of structures and the exploration of application means, etc. However, no matter active or passive elastic wave metasurfaces, a large number of research works are limited to the ordinary first-order diffraction, and the mechanism of elastic wave diffraction for higher-order diffraction has not been systematically studied.

Therefore, to address the above issues, the following works are done in this paper: 1. A new helical type metasurface is designed independently, and it is verified by simulation that the Lamb wave still fits the modified GSL, but it does not fit perfectly due to the multimodal and dispersion characteristics of the Lamb wave and the limitation of the structure itself. 2. Based on the modification principle, the helical type elastic wave metasurface structure is used to design and realize the Lamb wave nearly full-angle asymmetric transmission phenomenon, the separation of antisymmetric and symmetric modes and the waveguide structure. While verifying the universality of the correction theory in the field of elastic waves, it also provides an aid for the application of guided waves in the fields of nondestructive testing and architectural acoustics, and a new way for the fine processing of Lamb waves.

2 RELEVANT THEORIES AND MODEL CONSTRUCTION

2.1 Correlation Theory

If a phase gradient is introduced at the interface of two media through a metasurface, disrupting the original phase continuity at the interface, then the direction of the transmitted wave no longer satisfies Snell's law, but will follow the GSL proposed by Yu et al in 2011, written in the following form [4]:

$$k_1 \sin\theta_t - k_1 \sin\theta_i = \xi \tag{1}$$

Where, i, t subscripts denote the incident and transmitted; k_1 is the wave number of the incident wave and has $k_1 = 2\pi/\lambda_1$, λ_1 denotes the incident wave wavelength; ξ denotes the phase gradient, and $\xi = d\phi/dx$.

If the incident angle θ_i is larger than the critical angle θ_s (the critical angle will make $\sin\theta_t = 1$), it will produce the same diffraction phenomenon as the optical/acoustic grid structure, producing diffracted waves of different orders, as shown in **Figure 1A**. Thus, Xie et al. introduced the higher-order diffraction term into the classical GSL transmission law by analogy and induction, giving birth to a modified GSL based on the higher-order diffraction term, expressed in the following form [6]:

$$k_1 \sin\theta_t - k_1 \sin\theta_i = \xi + n_G G \tag{2}$$

Where G denotes the reciprocal vector, which is numerically the same as the phase gradient ξ, but is formed for different reasons, the former due to the periodic nature of the structure and the latter due to the discrete distribution of the transmitted phase; n_G is the higher order diffraction term, which takes the value of $n_G \in (0, -1, -2, ..., -N_G)$. In some recent articles, it is also expressed $1 + n_G$ as n, taking the value $n \in (1, 0, -1, -2, ..., -N)$, the phase gradient ξ and the reciprocal vector G are written in the form of numerical equality $\xi = G$, so that the above equation can be written as the following formula [30]:

$$k_1 \sin\theta_t - k_1 \sin\theta_i = n\xi \tag{3}$$

The physical meaning of the equation can be better illustrated by the wave vector diagram in **Figure 1B**. For each incident angle θ_i, the transmission angle can be found at the corresponding diffraction level. However, as the number of diffraction levels n increases, the incident wave angle θ_i cannot find the corresponding transmission angle in the wave number circles of the corresponding level even if it reaches the maximum value of 90°, as in the case of $n = -3$ in the figure. Therefore, for a specific spacing ξ (phase gradient, which is taken as $\xi = 2\pi/L$ in this paper) and radius of the wave number circle k_1 , the diffraction level n is taken to the highest order diffraction level $-N$. More precisely, the maximum diffraction level $-N$ is affected by the wavelength of the incident wave λ_1 and the length of a single period of the metasurface structure L, and substituting $|\sin\theta_t - \sin\theta_i| < 2$ into **Eq. 3** yields $N = roundup[-2k_1/G] + 1$. The equations related to wavelength and length are written as follows [7]:

$$N = roundup[-2L/\lambda_1] + 1 \tag{4}$$

Where $roundup$ is the upward rounding function.

However, not all of the sound waves will be transmitted along their respective diffraction channels, and Fu treats a unit cell in the metasurface structure as a Fabry-Perot resonator, as shown in **Figure 2**. When the angle θ_i of the incident wave is

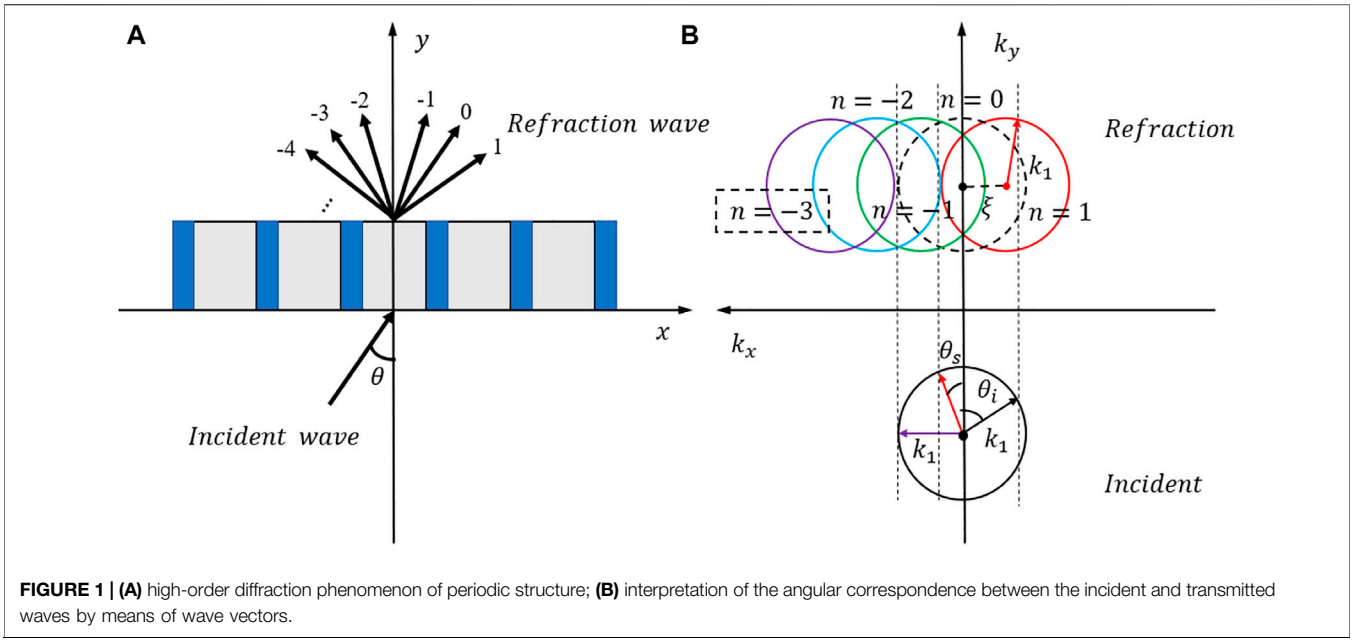

FIGURE 1 | (A) high-order diffraction phenomenon of periodic structure; **(B)** interpretation of the angular correspondence between the incident and transmitted waves by means of wave vectors.

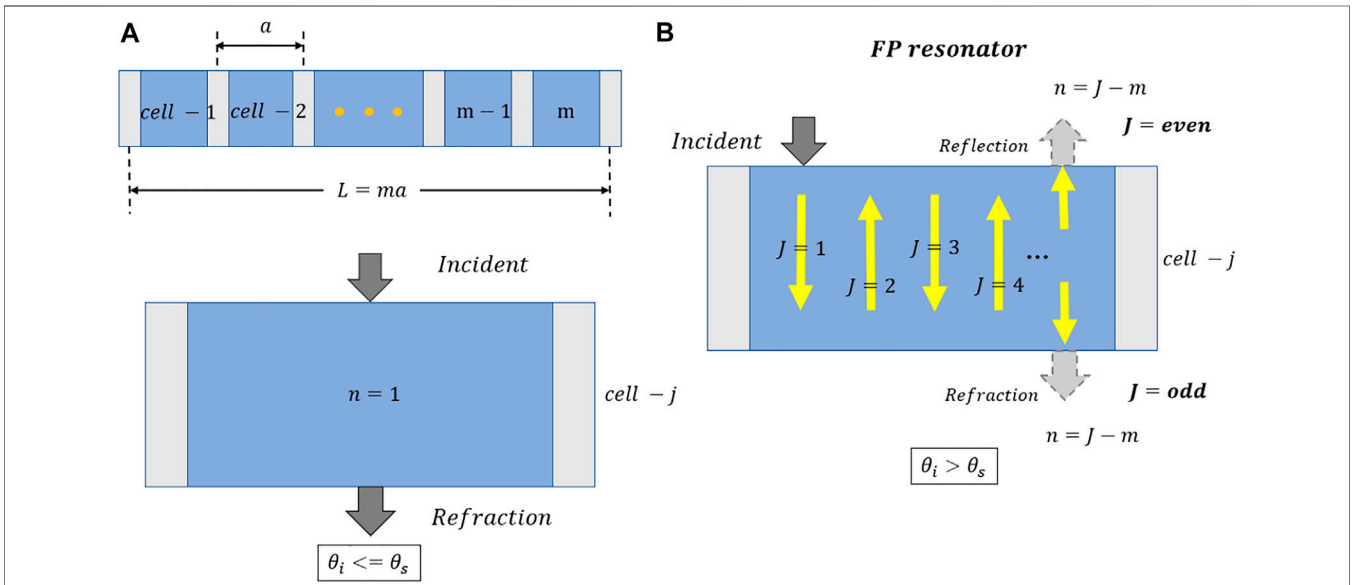

FIGURE 2 | (A) When the incident angle is less than or equal to the critical angle, the incident wave is transmitted normally from the unit cell; **(B)** When the incident angle is greater than the critical angle, the unit cell can be regarded as a Fabry-Perot resonator.

less than or equal to the critical angle θ_s, the incident wave will be transmitted directly from the diffraction channel $n = 1$; when θ_i is greater than the critical angle θ_s, multiple diffraction channels will be opened and the incident wave will be reflected back and forth in the unit cell until the accumulated wave path satisfies the condition before transmission or reflection occurs. It can be found that when the number of reflections J is odd, the incident wave passing through the metasurface interface behaves as transmission and otherwise it appears as reflection, both of which propagate directly from the diffraction channel of the nearest and largest diffraction level, because this channel represents the smallest wave path, so the energy propagated by the largest diffraction level tends to be the highest. And the reflection and transmission satisfy the GSL transmission and reflection formulas, respectively. In summary, the law can be succinctly expressed as the following **Eq. 7**:

$$k_1 \sin\theta_t - k_1 \sin\theta_i = nG \quad (J\ is\ odd) \tag{5}$$

$$k_1 \sin\theta_r - k_1 \sin\theta_i = nG \quad (J\ is\ even) \tag{6}$$

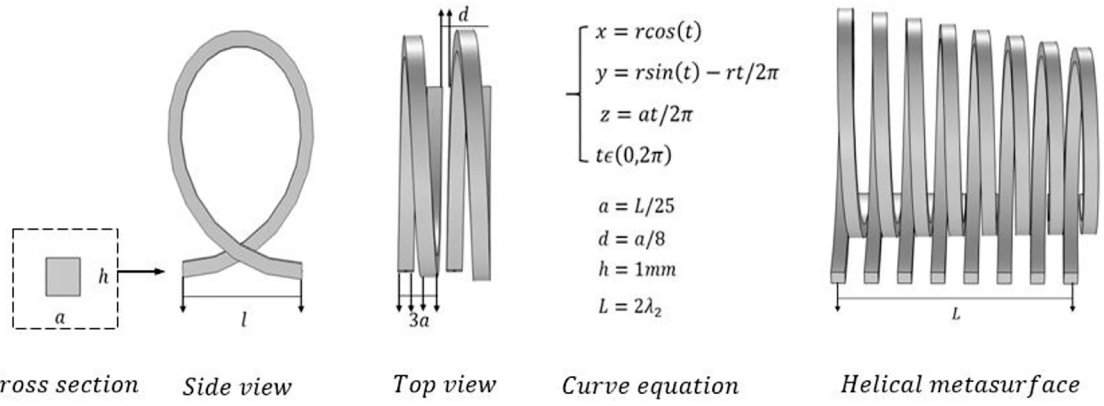

FIGURE 3 | Helical metasurface structural parameters.

where, $J = m + n$ represents the number of reflections, controlled by the number of unit cells m and the number of diffraction levels n. This equation shows that for a certain value of J, the transmission and reflection angles of incident light and sound waves in air can be accurately predicted when they pass through a periodically arranged metasurface structure, and are generally expressed mainly as transmitted or reflected waves at the corresponding maximum diffraction level. However, this equation only reveals the laws followed by the metasurface in regulating the acoustic waves, but there is no corresponding discussion for the complex elastic waves, which leads to a large number of existing theories for the study of elastic wave metasurfaces still stuck in the classical GSL, **Eq. 1**.

2.2 Design of a Helical Metasurface for Modulating Plate Waves

In this paper, we design a helical metasurface for modulating Lamb waves, which consists of a series of helical curved beam cells, as shown in **Figure 3**, where L indicates the length of a single cycle and l is the vertical span of the metasurface. The helical curved beam is formed by sweeping a rectangular section along the helical line, where the height of the rectangular section h is equal to the thickness of the sheet, which is 1 mm, and the length a is related to the number of unit cells. The parameter equation r is an adjustable parameter, and different values of r in the curve equation can be set to achieve different curved beam lengths. In order to maintain the continuity of the wave front when regulating the transmitted waves, the incident waves should have a phase difference of at least 2π, or generally a positive integer multiple of 2π, when they are transmitted from the first and last cells in the structure. In this paper, we construct $0 \sim 2\pi$ equal gradients of phase in the structure, so according to $d\varphi_i = k_2 ds_i$, we can invert the difference of the length between the curved beams (where φ is the phase, s is the wave path, subscript i indicates the curved beam number, and k_2 is the number of waves in the curved beam), and then according to the length integral equation $s_i = \int_0^{2\pi} \sqrt{[x'(t)]^2 + [y'(t)]^2 + [z'(t)]^2} dt$, can calculate and design the length of each helical line segment.

It is worth noting that the waves in the thin plate exist in the form of Lamb waves, while in the curved beam exist mainly in the form of bending waves, and there is a difference in the wave numbers between them. The wave numbers k_1 in **Eqs. 1–6** are the wave numbers of Lamb waves in A_0 mode, which can be obtained from the dispersion curves, while k_2 above is the wave number in the helical curved beam, which is obtained from the bending wave number equation $k_2 = \sqrt[4]{\rho S\omega^2/EI}$ [17], where ρ is the density, S is the area of the beam section, ω is the angular frequency of the excitation, and EI is the structural stiffness. At the same time, the curvature of this metasurface structure has a small rate of change, so it can maintain a high transmittance.

3 VERIFICATION OF MODIFIED GSL THEORY BASED ON HELICAL TYPE METASURFACE

In order to address the problem that a large number of elastic wave metasurfaces are still based on the GSL law which does not consider the higher order diffraction terms, this paper verifies the universality of the modified GSL theory by using the helical metasurface designed above.

Since the parity of the number of unit cells (actually, the number of equal parts of the 2π phase) mentioned in the modified GSL theory affects the diffraction phenomenon, the number of unit cells m in the structure of the metasurface is changed and the phases are redistributed according to the number, as follows: first, the length of the single cycle L of the metasurface is kept constant at one wavelength λ_1 , and the maximum diffraction level $-N$ can be calculated by **Eq. 4** at this time is -1, and the values of n are taken as (1, 0, -1). Further substitution into **Eq. 3** leads to the critical angle of $\theta_s = 0^\circ$. In order to control the variables as much as possible, the cross-sectional dimensions of each helical curved beam are kept the same, with both length and width $L/19$ and 1mm, and only the spacing between the curved beam cells d is changed, and the transmission phase difference of 2π is redistributed uniformly into each curved beam cell according to the changed parameter r. Finally, the metasurface structure

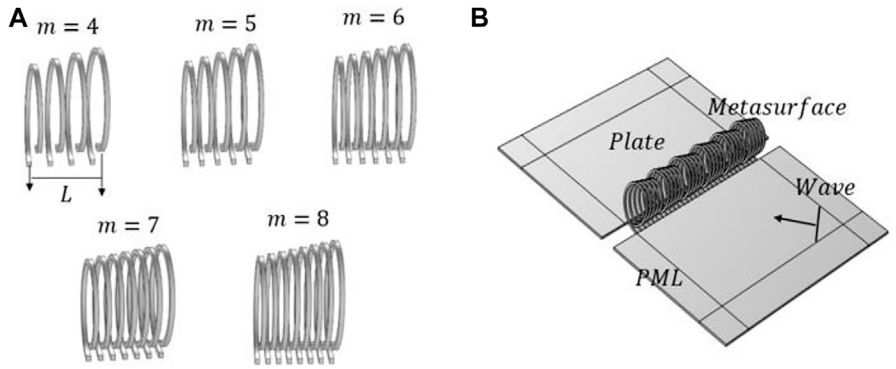

FIGURE 4 | (A) Helical metasurface structures with different numbers of unit cells; **(B)** Schematic diagram of the overall structure.

TABLE 1 | Values of phase φ, length s and parameters r corresponding to metasurfaces with different unit cell numbers after phase redistribution.

m	*e*	1	2	3	4	5	6	7	8
4	$\varphi_e/2\pi$	1/4	1/2	3/4	1	-	-	-	-
	s_e/λ_2	6 + 1/4	6 + 1/2	6 + 3/4	7	-	-	-	-
	r_e/λ_2	1.012	0.973	0.936	0.903	-	-	-	-
5	$\varphi_e/2\pi$	1/5	2/5	3/5	4/5	1	-	-	-
	s_e/λ_2	6 + 1/5	6 + 2/5	6 + 3/5	6 + 4/5	7	-	-	-
	r_e/λ_2	1.022	0.988	0.958	0.93	0.903	-	-	-
6	$\varphi_e/2\pi$	1/6	1/3	1/2	2/3	5/6	1	-	-
	s_e/λ_2	6 + 1/6	6 + 1/3	6 + 1/2	6 + 2/3	6 + 5/6	7	-	-
	r_e/λ_2	1.026	1	0.973	0.948	0.925	0.903	-	-
7	$\varphi_e/2\pi$	1/7	2/7	3/7	4/7	5/7	6/7	1	-
	s_e/λ_2	6 + 1/7	6 + 2/7	6 + 3/7	6 + 4/7	6 + 5/7	6 + 6/7	7	-
	r_e/λ_2	1.03	1	0.984	0.962	0.941	0.922	0.903	-
8	$\varphi_e/2\pi$	1/8	1/4	3/8	1/2	5/8	3/4	7/8	1
	s_e/λ_2	6 + 1/8	6 + 1/4	6 + 3/8	6 + 1/2	6 + 5/8	6 + 3/4	6 + 7/8	7
	r_e/λ_2	1.033	1.012	0.992	0.973	0.954	0.936	0.919	0.903

parameters with the values of 4, 5, 6, 7, and 8 for the number of unit cells m were obtained by the backpropagation calculation in the previous section. The structure schematic and parameters 12 are shown in **Figure 4A** and **Table 1**, respectively.

In our study, the commercial simulation software COMSOL is used to numerically simulate the phenomenon of controlling the plate wave transmission through the metasurface structure. Both the thin plate and the metasurface are made of aluminum, the elastic modulus is 70GPa, the Poisson's ratio is 0.33, and the density is 2700 kg/m̂3, and the excitation is set to a line excitation with a common ultrasonic excitation frequency of 100 kHz and an amplitude size of 1 mm. The metasurface structure is periodically arranged in the middle of the plate, and the overall structure is shown in **Figure 4B**.

When the Lamb wave is incident at −30° (the angle of incidence is less than the critical angle 0°), according to the above theoretical analysis, the number of unit cells does not affect the transmission because no higher-order diffraction waves are generated at this time. The simulation results are exactly the same, as shown in **Figure 5**. Although there are some unexpected reflections at $m = 5$, the overall solution is satisfied, and the transmission angle is not related to the number of unit cells m.

When the wave is incident in the direction of 30° (the angle of incidence is greater than the critical angle of 0°), higher order diffraction phenomenon will be generated at this time, where the maximum diffraction level $n_{\max} = -N = -1$, theoretically corresponding to the reflection or transmission angle according to **Eqs. 5**, **6** should be transmission angle −30°, reflection angle −30°, transmission angle −30°, reflection angle −30°, reflection angle −30°, respectively. The simulated wavefield as shown in **Figure 6**, and the transmitted or reflected wavefront basically satisfies this condition, except that an unexpected reflected wave is also generated at $m = 4$.

From **Eq. 4**, it can be seen that, without changing the wavelength of the incident wave, only increasing the length L, the other parameters of the metasurface structure remain unchanged, which will make the maximum diffraction level $-N$ larger and increase the channels of diffraction level n, so will the transmission of Lamb waves continue to satisfy the theory at this time? In order to answer this question, we set the length of

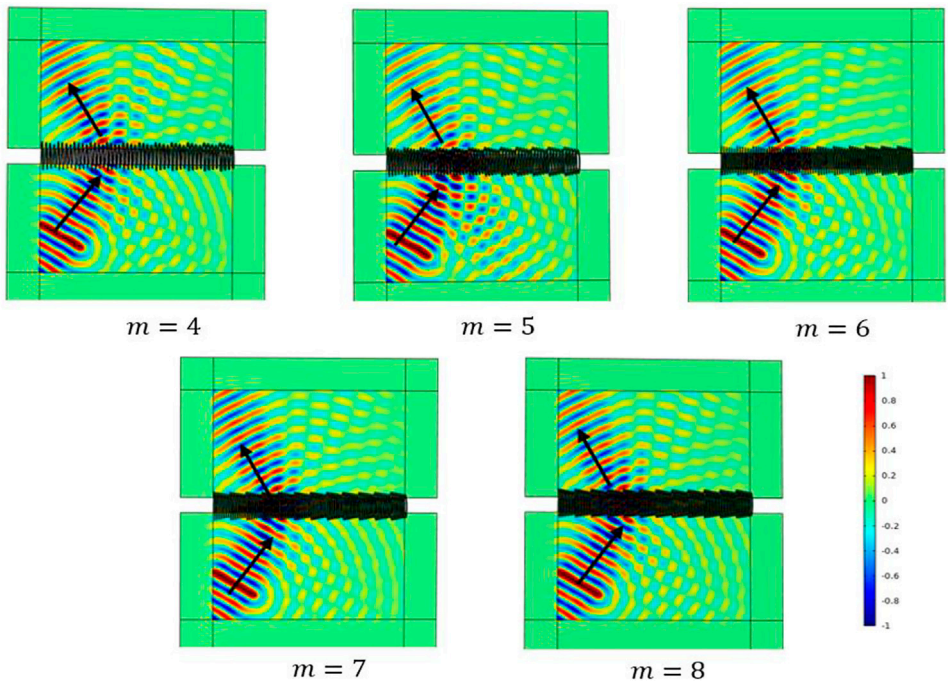

FIGURE 5 | When the incident angle is -30°, the corresponding transmission wavefields of metasurfaces with different unit cell numbers.

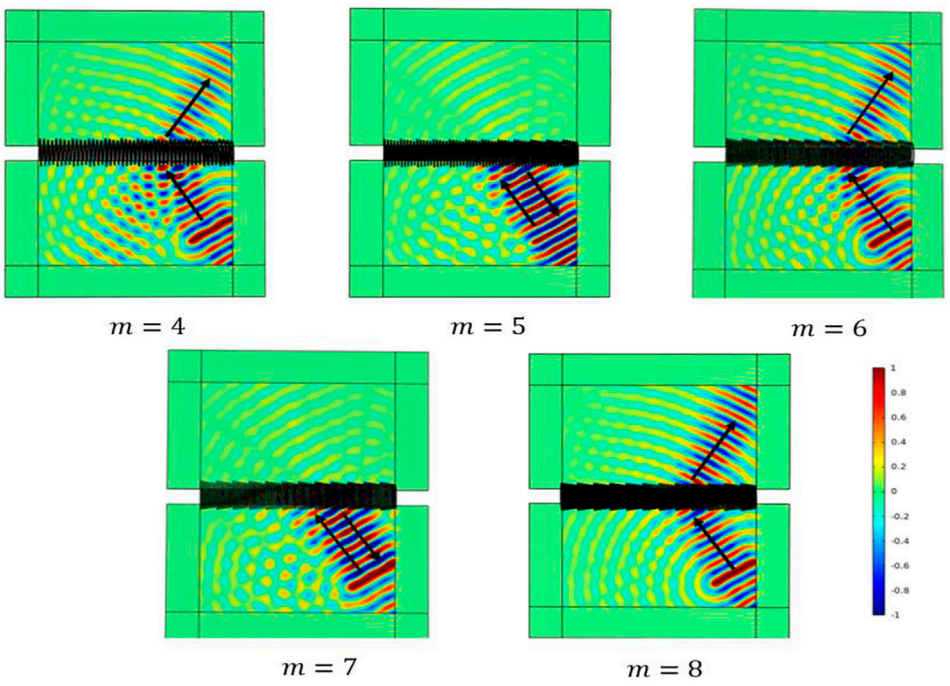

FIGURE 6 | When the incident angle is 30°, the corresponding transmission wavefields of metasurfaces with different unit cell numbers.

the single-period structure $L = 2\lambda_1$, and calculate the values of $N = 3$ and n as $(1, 0, -1, -2, -3)$ from **Eq. 4**, then substitute it into **Eq. 5** can get the critical angle of 30°. If 30° is still chosen as the angle of incidence, no higher order diffraction is produced, so we reset the incident angle of 45°. The simulation results are shown in **Figure 7**. When m is an even number, there is a clear

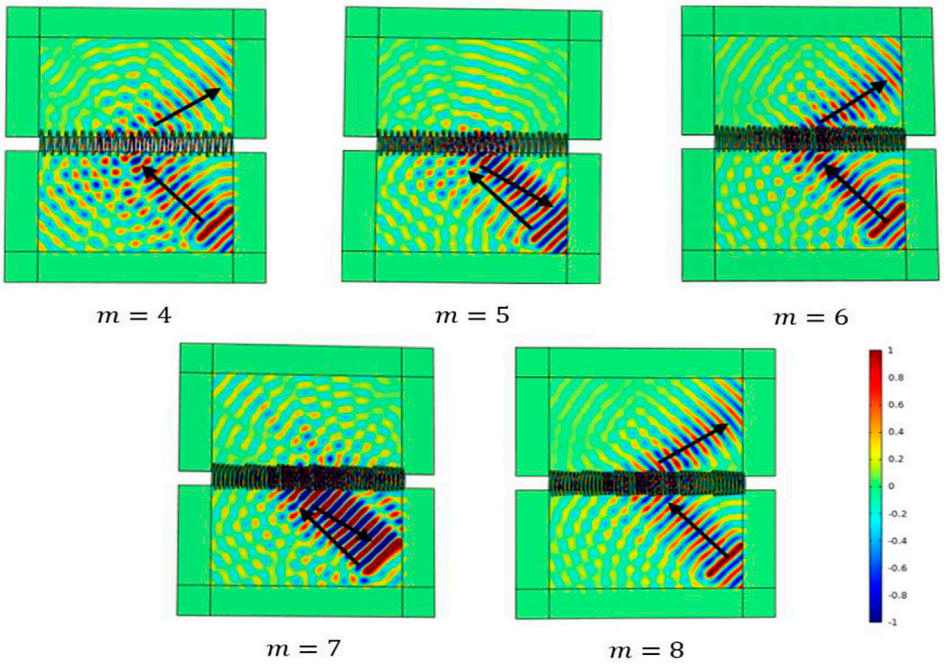

FIGURE 7 | When $L = 2\lambda_1$, the incident wave angle is 45°, the corresponding transmitted wavefields of metasurfaces with different unit cell numbers.

transmission phenomenon, and the transmission angle is close to the theoretical value of −52.5° calculated by **Eq. 6**. Although there are still reflected waves at $m = 4$, the concentration of transmitted energy to the highest level $n = -3$ gradually appears as the number of unit cells m increases. On the other hand, the anomalous reflection occurs at an odd number of m, and the reflection angle is also −52.5°, similarly, the reflected energy is enhanced as the number of unit cells increases. It can be concluded that regardless of the value of L and the number of diffraction levels n, as long as the incident angle is greater than the critical angle, the main energy of the incident Lamb wave passing through the interface will jump directly to the highest diffraction level and appear as a reflected or transmitted wave.

In conclusion, Lamb wave also conforms to the modified diffraction law to some extent, but the existence of multi-mode and dispersion in the guided wave, or the problem of the structure itself, lead to weak reflection and transmission energy in other diffraction channels.

4 ACOUSTIC APPLICATIONS BASED ON MODIFIED GSL THEORY

4.1 Negative Refraction and Asymmetric Transmission of Lamb Waves at Nearly all Angles

According to the theory in the previous section, if set $L = \lambda_1$, the highest diffraction order is −1 and the critical angle is 0°. When the incident angle is greater than 0° and the number of unit cells in the structure is an even number, that is, when the number of reflections $J = m + n$ is an odd number, the high-order diffracted wave behaves as a transmitted wave at this time, which satisfies **Eq. 6**, and can be written as follows by substituting $L = \lambda_1$ and $n = -1$ into it form:

$$\sin\theta_t - \sin\theta_i = -1 \quad (\theta_i > 0) \tag{7}$$

When the incident angle is less than or equal to 0°, it conforms to the classical GSL. Substitute $L = \lambda_1$ and $n = 1$ into (1.6) to get:

$$\sin\theta_t - \sin\theta_i = 1 \quad (\theta_i \leq 0) \tag{8}$$

Combining **Eqs. 7**, **8**, it can be seen that when the two incident wave directions are symmetric about the vertical axis, the transmitted wave directions will also behave as axisymmetric, and the incident wave angle will always remain opposite in sign to the transmitted angle (except for 0°). This also indicates that it is theoretically possible to achieve nearly full-angle negative refraction except for the incident angle of 0°. Therefore, in this paper, the number of unit cells is set to $m = 8$, and the detailed parameters of the structure are shown in **Table 1**. The incident waves are incident at + -30°, +-45°, and +-60°, respectively, with the same excitation mode and frequency, and the simulation results are obtained as shown in **Figure 8**. It can be found that the wave field in the figure is exactly the same as the theoretical prediction. When the incident wave is incident at positive and negative angles, the transmitted wave is also transmitted at corresponding angles of -+30°, -+17°, and -+7.7°, respectively, and the sign is opposite to the incident angle, realizing a perfect wide-angle negative refraction phenomenon.

As an important acoustical phenomenon, asymmetric transmission enables unidirectional wave transmissibility,

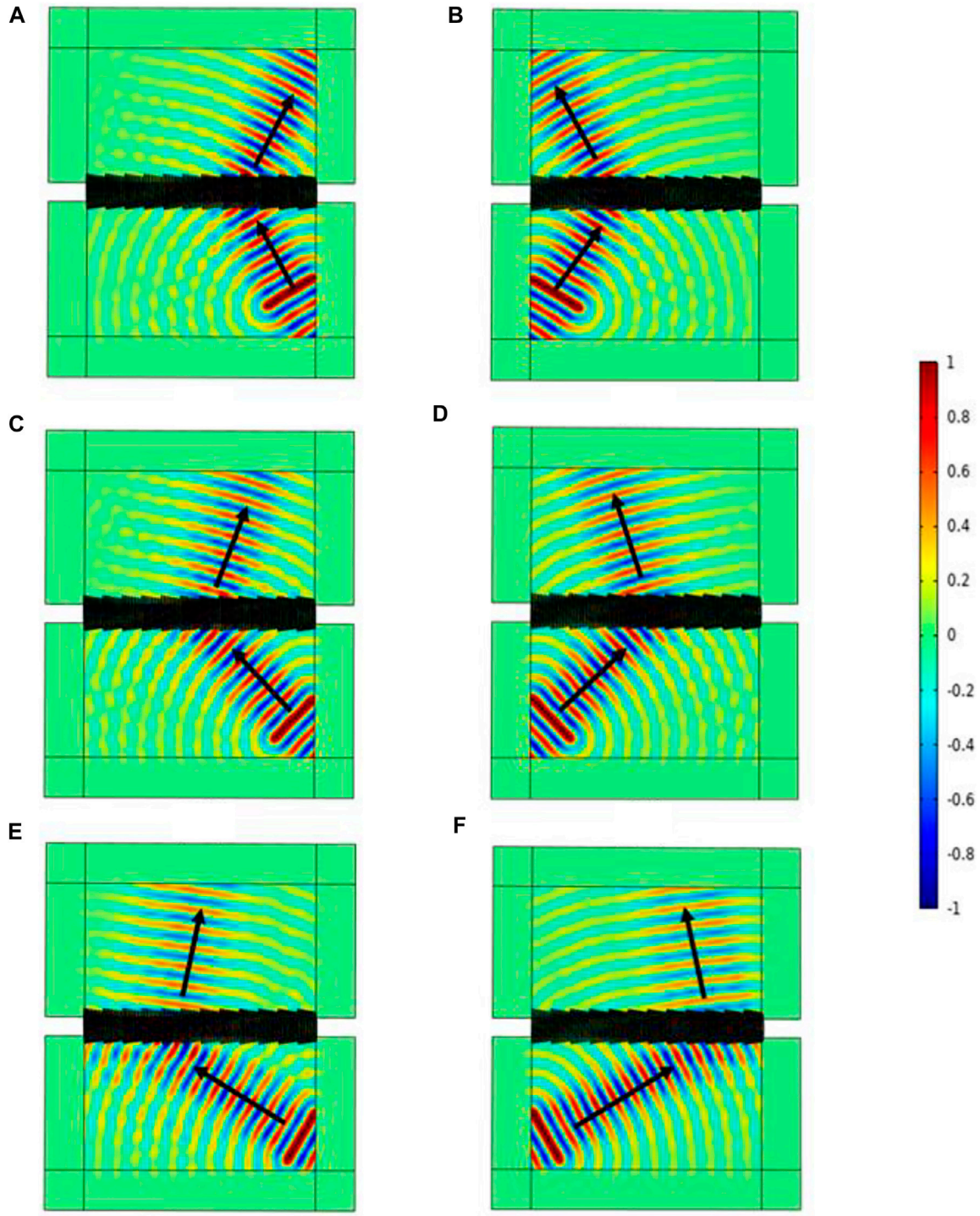

FIGURE 8 | Wide-angle negative refraction phenomenon of the incident waves: **(A)** 30°; **(B)** -30°; **(C)** 45°; **(D)** -45°; **(E)** 60°; **(F)** -60°.

waves can propagate from one side to the other side of the interface, while they cannot transmit from the reverse direction, such phenomena have great potential for application. In the field of elastic waves, the asymmetric transmission of waves can also be realized by metasurface structures. Therefore, in this paper, an asymmetric transmission device is designed based on the theory of parity-related diffraction, which only allows the single-pass of waves and perfectly realizes the wide-angle asymmetric transmission of Lamb waves.

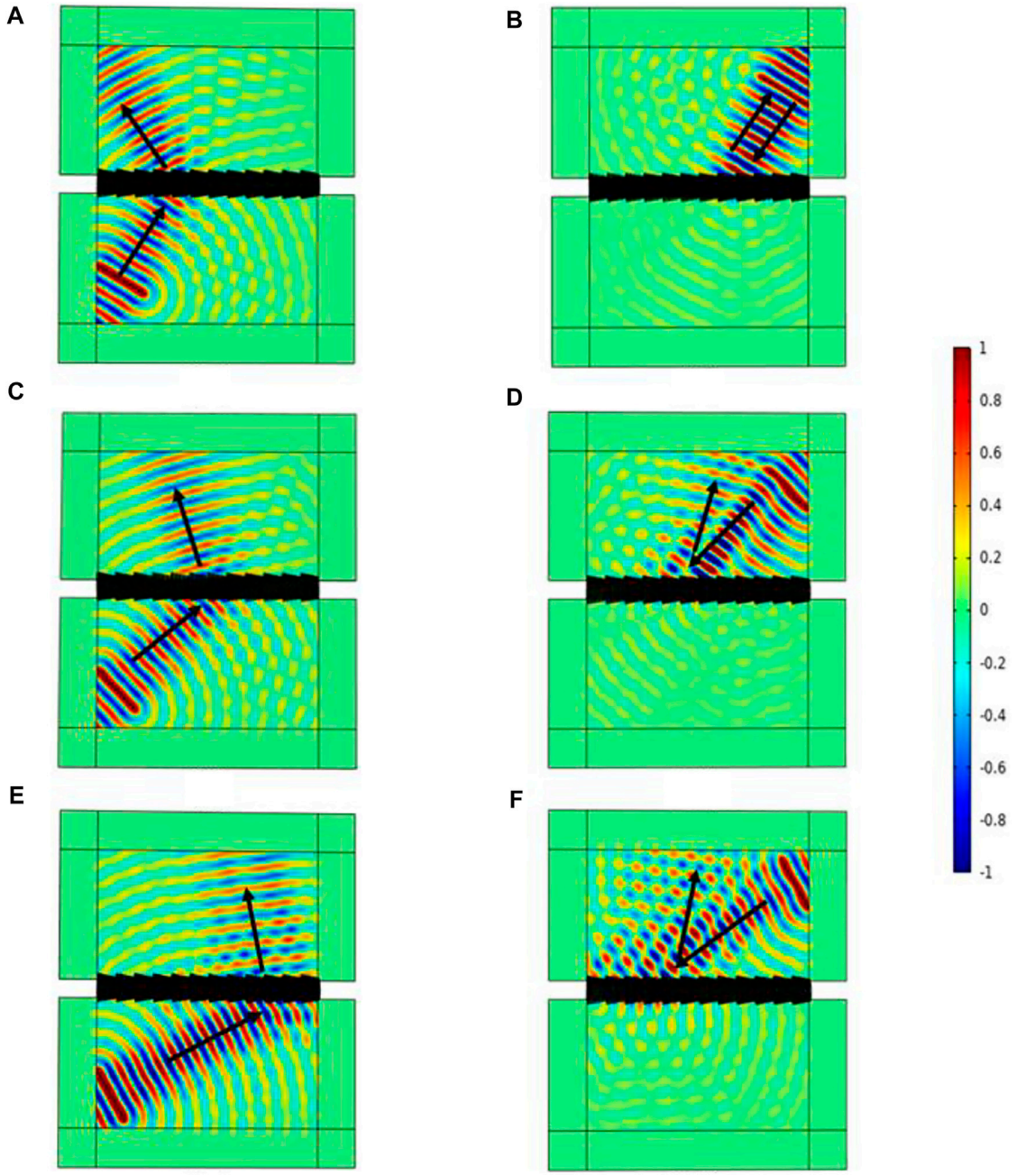

FIGURE 9 | Wide-angle asymmetric transmission of incident waves: **(A)** lower left corner -30° **(B)** upper right corner 30°; **(C)** lower left corner -45° **(D)** upper right corner 45°; **(E)** lower left corner - 60°**(F)** 60° to the upper right corner.

Setting $L = \lambda_1$, at this time, based on the parity-related diffraction theory **Eqs. 7**, **8**, it is known that if the number of unit cells m is designed as odd and $m + n$ as even, the higher-order diffracted wave will be reflected when the incident wave angle is greater than the critical angle 0°, and the reflection angle satisfies **Eq. 6**. Therefore, when the waves are incident in opposite directions from the lower left and upper right angles, respectively, the transmission is not the same, resulting in an asymmetric propagation path of Lamb waves.

Therefore, the number of unit cells is set to $m = 7$, and the parameters are shown in **Table 1**, and the rest of the settings are the same as above, and then the simulation results are obtained when the waves are incident at −30°, −45°, −60° at the lower left corner and 30°, 45°, 60° at the upper right corner, respectively, as shown in **Figure 9**. By comparison, it is found that the wave fields in the figure possess good asymmetry, and the transmission directions are 30°, 17° and 7.7°, and the reflection directions are −30°, −17° and −7.7°, and the two groups of wave fields

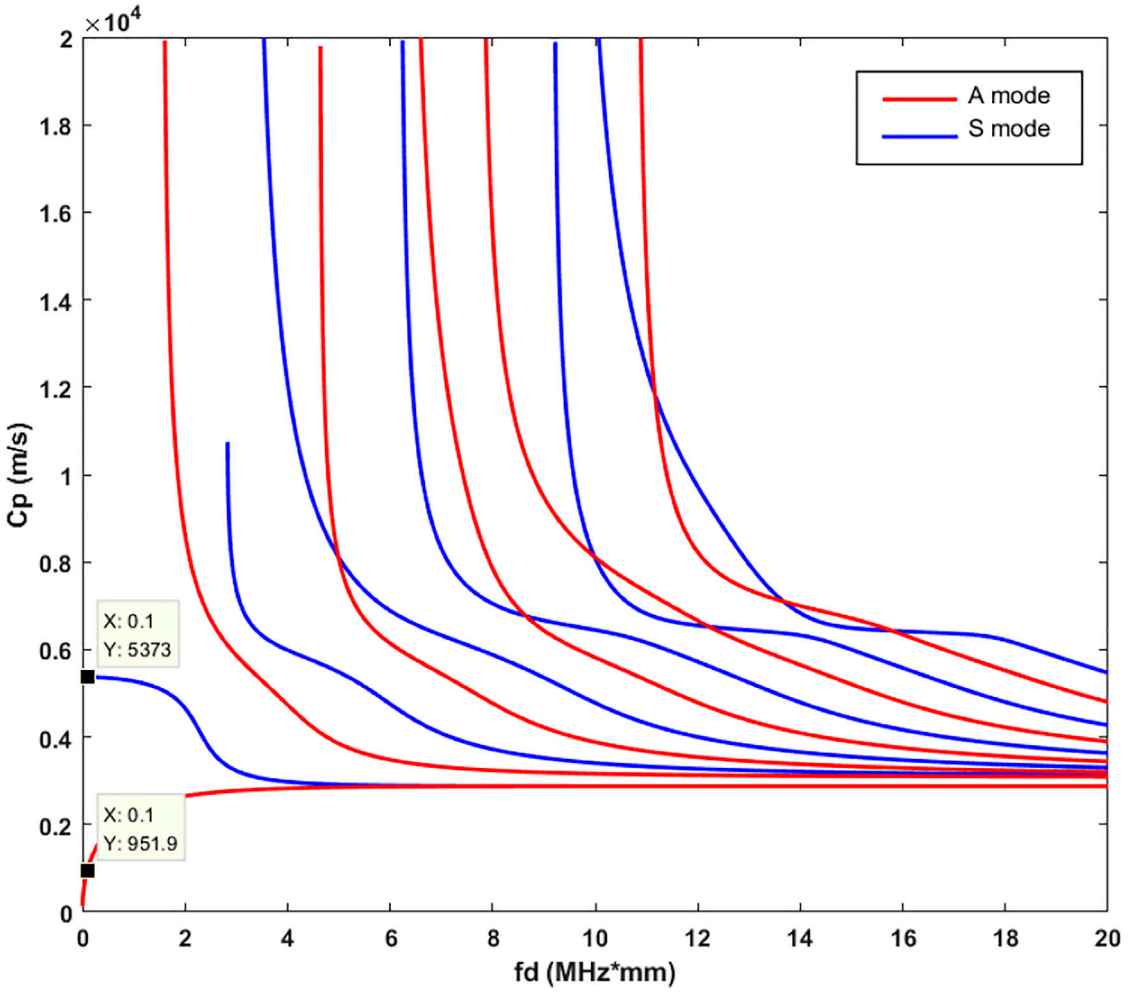

FIGURE 10 | Dispersion curve of aluminum plate.

form a perfect asymmetric transmission phenomenon with each other.

4.2 Modal Separation of Lamb Waves

When Lamb waves are used for structural damage monitoring, they often cause wave packet mixing because they have multiple modes, which further causes the damage signal to be difficult to identify and the problem of inaccurate damage imaging. How to separate the different modes of Lamb waves quickly and accurately is one of the important problems in the field of structural health monitoring that needs to be solved.

In this section, based on the difference of wave velocities between symmetric mode (S) and antisymmetric mode (A) of Lamb wave, a simple mode separator is constructed based on the parity-related diffraction theory, and the separation of A_0 mode and S_0 mode waves at an excitation frequency of 100 kHz is initially realized.

First, the aluminum plate dispersion curve was plotted, as shown in **Figure 10**. According to this figure, the wave velocities of A_0 mode and S_0 mode wave at the frequency thickness product of 100 kHz*1 mm are 951.9 m/s and 5373 m/s, respectively, in other words, the wavelength of S_0 mode wave at this frequency is 5.6 times that of A_0, $\lambda_3 = 5.6\lambda_1$ and only A_0 and S_0 mode waves exist at this frequency thickness product.

Second, according to the parity-related diffraction theory and **Eq. 4**, it is known that for the S_0 mode, $\lambda_0 = 5.6\lambda_1$ in this equation, the maximum diffraction level $-N$ can only be 0 when $L = 1.1\lambda_1$, and **Eqs. 5**, **6** are then rewritten as

$$\sin\theta_t - \sin\theta_i = 0 \quad (J\,is\,odd) \tag{9}$$

$$\sin\theta_r - \sin\theta_i = 0 \quad (J\,is\,even) \tag{10}$$

The above equation shows that the transmission or reflection angle is equal to the incidence angle when the S_0 mode wave at this frequency thickness product is incident in any direction. However, for the A_0 mode wave, when it is incident vertically in the 0° direction, it satisfies the classical GSL **Eq. 1**, with a theoretical transmission angle of 65.4°. In order to illustrate the effect of mode separation when Lamb wave field is excited in three cases: 1. A_0 mode (control group) 2. A_0 and a few S_0

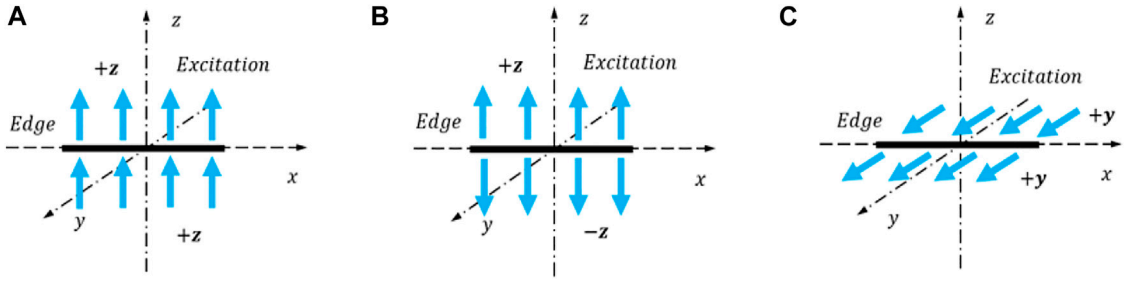

FIGURE 11 | Three types of excitation: **(A)** Antisymmetric excitation about the *xy* plane; **(B)** symmetric excitation; **(C)** antisymmetric excitation about the *xz* plane.

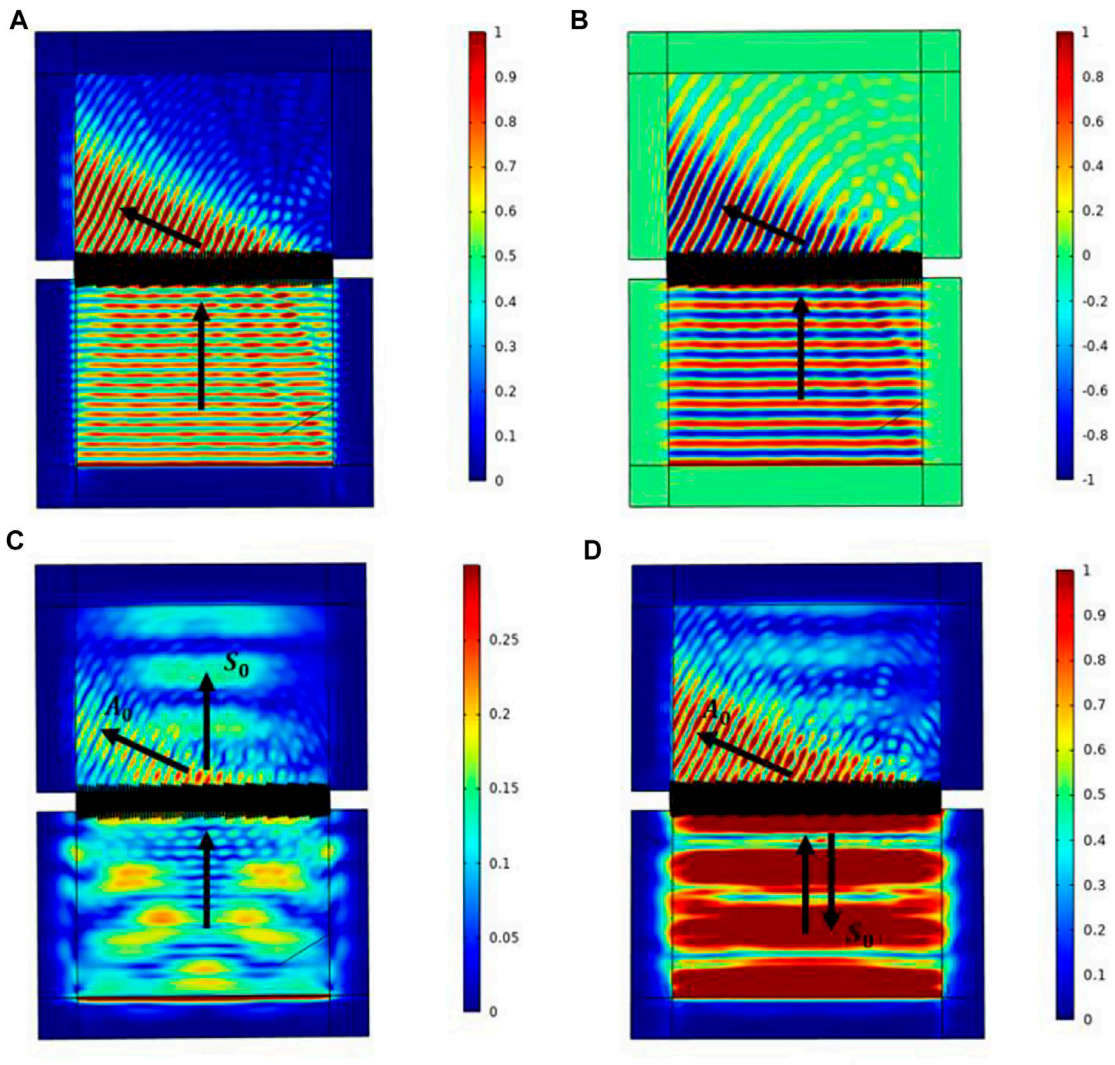

FIGURE 12 | (A) Total displacement corresponding to the first excitation method (combined plot of displacements in three directions); **(B)** z-directional displacement (off-plane displacement); **(C)** total displacement corresponding to the second excitation method; **(D)** total displacement wavefield corresponding to the third excitation method.

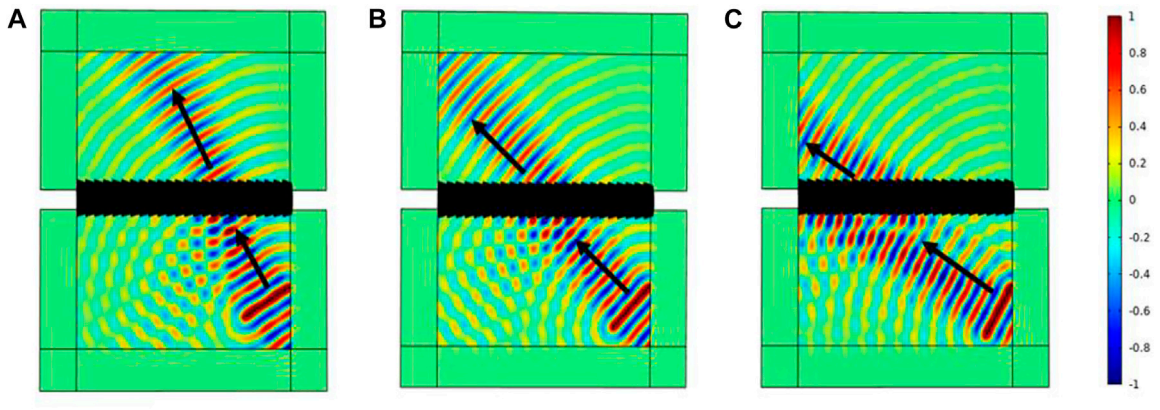

FIGURE 13 | When the number of unit cells is m = 7, the wave field of the incident wave incident at different angles: **(A)** 30°; **(B)** 45°; **(C)** 60°.

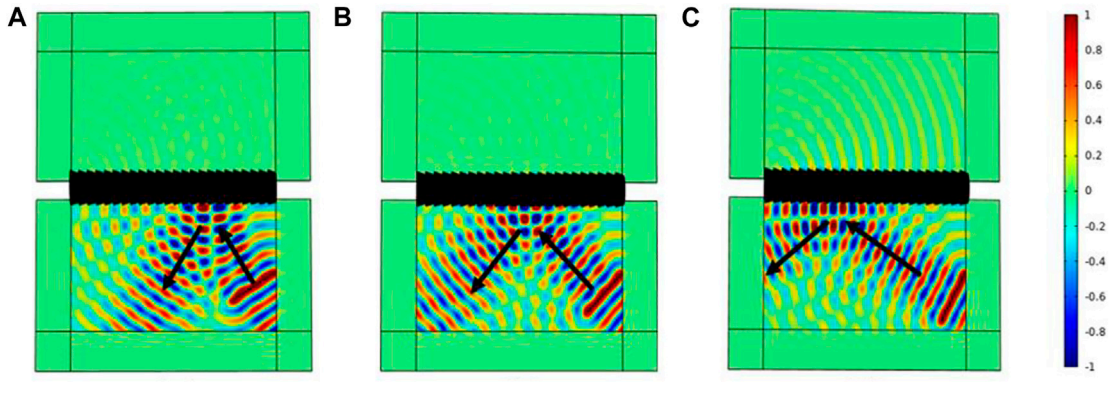

FIGURE 14 | When the number of unit cells is m = 8, the wave field of the incident wave incident at different angles: **(A)** 30°; **(B)** 45°; **(C)** 60°.

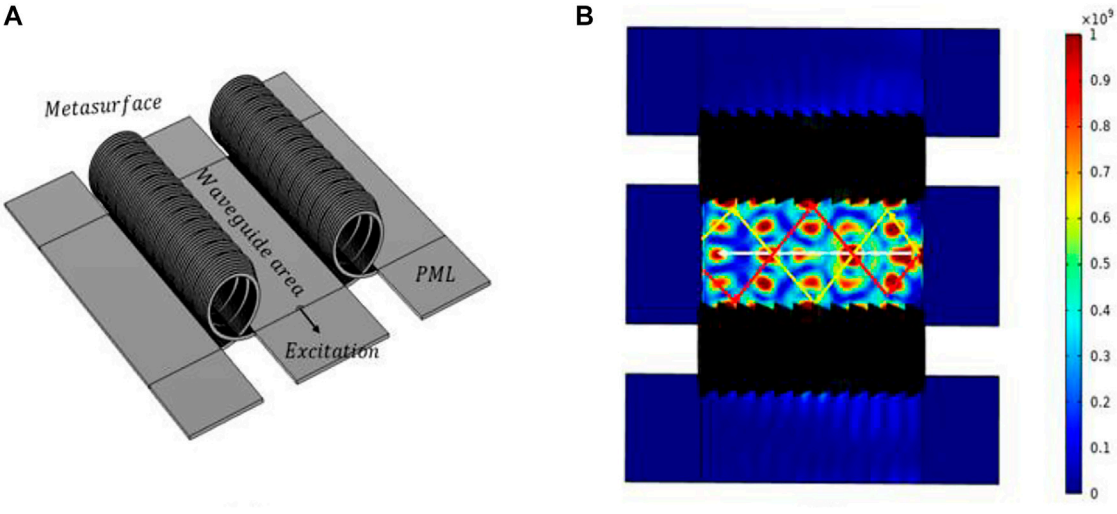

FIGURE 15 | (A) Schematic diagram of metasurface waveguide structure; **(B)** energy density diagram of Lamb wave propagating in the waveguide region.

modes 3. S_0 and a few A_0 modes, three excitations are selected in this section based on the principle that symmetric (S) and antisymmetric (A) modes are dominated by in-plane and off-plane displacements, respectively: (a) antisymmetric excitation about the *xy* plane (b) symmetric excitation (c) antisymmetric excitation about the *xz* plane, and the schematic diagram is shown in **Figure 11**.

Then the first excitation method (a) is chosen, the excitation frequency is selected as 100 kHz, the amplitude size is 1 mm so that the structure length of the single-cycle metasurface $L = 1.1\lambda_1$, the number of unit cells m = 7, J is odd, and the rest of the settings remain unchanged, the total displacement wavefield is obtained as shown in **Figure 12A**, it can be clearly seen that the wavefield contains only a single mode wave. Comparing with the *z*-direction displacement wavefield in figure (b), it can be seen that the total displacement wavefield basically exists only in the z-directional off-plane displacement, and it is judged as A_0 mode according to the wavelength.

Next, the second excitation method (b) is adopted, about z-directional symmetric excitation, which can excite part of the S_0 mode wave. The theoretical analysis in this subsection shows that when the wave is incident at 0°, the A_0 wave will transmit at 65.4°, while the S_0 wave will maintain 0° transmission, and the two transmission directions are different, forming the beam separation phenomenon. The simulation results are shown in **Figure 12C**, and it can be found that the Lamb wave field in the figure achieves a mode separation phenomenon consistent with the theory, with the shorter wavelength being the A_0 wave and the opposite being the S_0, and the deflection angle is also consistent with the theoretical prediction.

Finally, the third excitation method is used, which can excite the S_0 mode with mainly in-plane displacement (*y*-direction displacement). The rest of the settings remain unchanged, and only the number of unit cells m is changed to 8, J is an even number. According to (1.10), most of the energy of the S_0 wave will be reflected, while the A_0 wave is still deflected in the direction of 65.4° after passing through the metasurface. The simulation results are shown in **Figure 12D**, which clearly shows the accuracy of the theoretical prediction and also achieves a more perfect separation of the two modes in Lamb waves.

In conclusion, this section designs this metasurface structure as a simple mode separator based on the parity-related diffraction theory, combined with the difference in the wavelengths of Lamb wave A_0 and S_0 modes. Moreover, a reasonable size can be designed based on the above theory to realize the separation of multiple modal waves of Lamb waves in any direction according to the actual needs.

4.3 Lamb Waveguide Structure

Similar to the case of S_0 wave propagation in the previous section, it is known from **Eq. 4** that when $L \leq \lambda_1/2$, the higher order diffracted waves of A_0 mode can only be coupled to level 0, the maximum diffraction level $-N = 0$. Therefore, when m is odd and even, respectively, the incident wave will also satisfy **Eqs. 9**, **10** with the same angular magnitude as the transmitted or reflected wave. Thus, a waveguide structure is designed in this section based on the full-angle total reflection phenomenon in it. This structure not only prevents the wave from leaking out, but also prohibits the wave from transmitting to the inside of the structure from the outside, forming a kind of "cage" to imprison the wave.

First, set $L \leq \lambda_1/2$, the number of unit cells m to 7, and the rest of the settings remain unchanged. The incident wave angles are still set to 30°, 45° and 60°, and the simulation results are shown in **Figure 13**. It can be seen that the waves in Figs. (a), (b) and (c) are transmitted at the same angle as the incident direction, which is the same as the results of the theoretical analysis.

Then set m to 8, and the rest of the settings remain unchanged. The simulation results are shown in **Figure 14**, and it can be found that the wave fields in Figs. (a), (b) and (c) are exactly as expected from the theory, and total reflection occurs in all of them, and total reflection occurs when the wave is incident at any angle in theory.

Based on the above discussion, a waveguide structure is designed by using this total reflection phenomenon. The structure schematic is shown in **Figure 15A**, which consists of two layers of the metasurface, and the middle range is the waveguide area. A line excitation is applied on the small semicircular edge, and the excitation waves in different directions will reflect back and forth when they encounter the metasurface interface, thus achieving directional propagation. Considering the large amount of computation of the metasurface model, the width of the middle waveguide region is set to be narrower and the length is shorter. The final energy density diagram is shown in **Figure 15B**. Although the Lamb wave is essentially leak-free, the conduction region is too small, resulting in a difficult to distinguish the wave path when it propagates inside the waveguide. Even so, the idea of using the metasurface as a waveguide structure is still feasible. If the metasurface structure can be simplified and the waveguide region can be designed from straight lines to curves or loops, then better conduction and isolation effects of Lamb waves can be further achieved.

5 CONCLUSION

The modified GSL theory is introduced in this paper for the higher-order diffraction phenomena are often neglected in elastic wave metasurfaces. While verifying its correctness by using helical type metasurfaces, a series of acoustic phenomena and applications are also realized by this theory. The details are as follows:

By introducing the concept of phase gradient, and based on the plate - beam elastic wave propagation theory, a helical type metasurface is constructed. It is verified through this structure that the parity-related diffraction theory is still applicable in the field of elastic waves, and the theory is well conformed even when the number of diffraction levels is large.

According to the modified GSL theory, negative refraction and asymmetric transmission at nearly all angles (except 0°), separation of symmetric and anti-symmetric modes in Lamb waves, waveguide structure with directional transmission function are designed and realized. It is shown that the theory

can not only improve the classical GSL law and play a better guiding significance, but also can realize some special functions in combination with the metasurface structure, which contains great potential for application in the fields of nondestructive testing and vibration noise control.

DATA AVAILABILITY STATEMENT

The original contributions presented in the study are included in the article/Supplementary Material, further inquiries can be directed to the corresponding author.

AUTHOR CONTRIBUTIONS

HY: Writing—original draft, Conceptualization, Methodology, Software, Data curation, Review of writing, editing, Visualization, Investigation. KF: structural scheme design and theoretical model analysis Funding acquisition, Formal analysis, Project administration, Review of writing, editing. RL: Supervision, Validation. JY: Visualization, Validation.

FUNDING

The project was supported by the National Natural Science Foundation of China (Grant no. 11702118), the Natural Science Foundation of Jiangsu Province (Grant no. BK20170520), and the Basic Research Program of Jiangsu Education Department (Grant no. 17KJB130005).

ACKNOWLEDGMENTS

We acknowledge the National Natural Science Foundation of China and the Natural Science Foundation of Jiangsu Province for their support.

REFERENCES

1. Ma G, Yang M, Xiao S, Yang Z, Sheng P. Acoustic Metasurface with Hybrid Resonances. *Nat Mater* (2014) 13(9):873–8. doi:10.1038/nmat3994
2. Assouar B, Liang B, Wu Y, Li Y, Cheng J-C, Jing Y. Acoustic Metasurfaces. *Nat Rev Mater* (2018) 3(12):460–72. doi:10.1038/s41578-018-0061-4
3. Wang Z, Chu Y. Research Progress of Acoustic Metasurface in China. *EPJ Appl Metamat* (2019) 6:5. doi:10.1051/epjam/2019004
4. Yu N, Genevet P, Kats MA, Aieta F, Tetienne J-P, Capasso F, et al. Light Propagation with Phase Discontinuities: Generalized Laws of Reflection and Refraction. *Science* (2011) 334(6054):333–7. doi:10.1126/science.1210713
5. Li Y, Liang B, Gu ZM, Zou XY, Cheng JC. Reflected Wavefront Manipulation Based on Ultrathin Planar Acoustic Metasurfaces. *Sci Rep* (2013) 3(1):2546. doi:10.1038/srep02546
6. Xie Y, Wang W, Chen H, Konneker A, Popa BI, Cummer SA. Wavefront Modulation and Subwavelength Diffractive Acoustics with an Acoustic Metasurface. *Nat Commun* (2014) 5(1):5553. doi:10.1038/ncomms6553
7. Fu Y, Shen C, Cao Y, Gao L, Chen H, Chan CT, et al. Reversal of Transmission and Reflection Based on Acoustic Metagratings with Integer Parity Design. *Nat Commun* (2019) 10(1):2326. doi:10.1038/s41467-019-10377-9
8. Zhu H, Semperlotti F. Anomalous Refraction of Acoustic Guided Waves in Solids with Geometrically Tapered Metasurfaces. *Phys Rev Lett* (2016) 117(3):034302. doi:10.1103/PhysRevLett.117.034302
9. Liu Y, Liang Z, Liu F, Diba O, Lamb A, Li J. Source Illusion Devices for Flexural Lamb Waves Using Elastic Metasurfaces. *Phys Rev Lett* (2017) 119(3):034301. doi:10.1103/PhysRevLett.119.034301
10. Yuan S-M, Chen A-L, Wang Y-S. Switchable Multifunctional Fish-Bone Elastic Metasurface for Transmitted Plate Wave Modulation. *J Sound Vibration* (2020) 470:115168. doi:10.1016/j.jsv.2019.115168
11. Yaw Z, Zhou W, Chen Z, Lim CW. Stiffness Tuning of a Functional-Switchable Active Coding Elastic Metasurface. *Int J Mech Sci* (2021) 207:106654. doi:10.1016/j.ijmecsci.2021.106654
12. Zhang S, Shu S, Bian X. Tunability for Anomalous Refraction of Flexural Wave in a Magneto-Elastic Metasurface by Magnetic Field and Pre-Stress. *Appl Phys Express* (2022) 15:027003. doi:10.35848/1882-0786/ac4925
13. Li S, Xu J, Tang J. Tunable Modulation of Refracted Lamb Wave Front Facilitated by Adaptive Elastic Metasurfaces. *Appl Phys Lett* (2018) 112(2):021903. doi:10.1063/1.5011675
14. Qiu H, Li F. Manipulation of Shear Horizontal Guided Wave with Arbitrary Wave Fronts by Using Metasurfaces. *J Phys D: Appl Phys* (2020) 53(28):285301. doi:10.1088/1361-6463/ab850d
15. Ruan Y, Liang X, Hu C. Retroreflection of Flexural Wave by Using Elastic Metasurface. *J Appl Phys* (2020) 128(4):045116. doi:10.1063/5.0005928
16. Zheng M, Park CI, Liu X, Zhu R, Hu G, Kim YY. Non-Resonant Metasurface for Broadband Elastic Wave Mode Splitting. *Appl Phys Lett* (2020) 116(17):171903. doi:10.1063/5.0005408
17. Zhang J, Zhang X, Xu F, Ding X, Deng M, Hu N, et al. Vibration Control of Flexural Waves in Thin Plates by 3D-Printed Metasurfaces. *J Sound Vibration* (2020) 481:115440. doi:10.1016/j.jsv.2020.115440
18. Chen Y, Li X, Hu G, Haberman MR, Huang G. An Active Mechanical Willis Meta-Layer with Asymmetric Polarizabilities. *Nat Commun* (2020) 11(1):3681. doi:10.1038/s41467-020-17529-2
19. De Ponti JM, Colombi A, Ardito R, Braghin F, Corigliano A, Craster RV. Graded Elastic Metasurface for Enhanced Energy Harvesting. *New J Phys* (2020) 22(1):013013. doi:10.1088/1367-2630/ab6062
20. Cao L, Yang Z, Xu Y, Chen Z, Zhu Y, Fan S-W, et al. Pillared Elastic Metasurface with Constructive Interference for Flexural Wave Manipulation. *Mech Syst Signal Process* (2021) 146:107035. doi:10.1016/j.ymssp.2020.107035
21. Lee SW, Shin YJ, Park HW, Seung HM, Oh JH. Full-Wave Tailoring between Different Elastic Media: A Double-Unit Elastic Metasurface. *Phys Rev Appl* (2021) 16(6):064013. doi:10.1103/physrevapplied.16.064013
22. Li B, Hu Y, Chen J, Su G, Liu Y, Zhao M, et al. Efficient Asymmetric Transmission of Elastic Waves in Thin Plates with Lossless Metasurfaces. *Phys Rev Appl* (2020) 14(5):054029. doi:10.1103/physrevapplied.14.054029
23. Jin Y, Wang W, Khelif A, Djafari-Rouhani B. Elastic Metasurfaces for Deep and Robust Subwavelength Focusing and Imaging. *Phys Rev Appl* (2021) 15(2):024005. doi:10.1103/physrevapplied.15.024005
24. Lin Z, Xu W, Xuan C, Qi W, Wang W. Modular Elastic Metasurfaces with Mass Oscillators for Transmitted Flexural Wave Manipulation. *J Phys D: Appl Phys* (2021) 54(25):255303. doi:10.1088/1361-6463/abee47
25. Ruan Y, Liang X. Reflective Elastic Metasurface for Flexural Wave Based on Surface Impedance Model. *Int J Mech Sci* (2021) 212:106859. doi:10.1016/j.ijmecsci.2021.106859

26. Kim MS, Lee WR, Kim YY, Oh JH. Transmodal Elastic Metasurface for Broad Angle Total Mode Conversion. *Appl Phys Lett* (2018) 112(24):241905. doi:10.1063/1.5032157
27. Xia R, Yi J, Chen Z, Li Z. *In Situ* steering of Shear Horizontal Waves in a Plate by a Tunable Electromechanical Resonant Elastic Metasurface. *J Phys D: Appl Phys* (2019) 53(9):095302. doi:10.1088/1361-6463/ab5cbc
28. Zhu H, Patnaik S, Walsh TF, Jared BH, Semperlotti F. Nonlocal Elastic Metasurfaces: Enabling Broadband Wave Control via Intentional Nonlocality. *Proc Natl Acad Sci U.S.A* (2020) 117(42):26099–108. doi:10.1073/pnas.2004753117
29. Xu Y, Cao L, Yang Z. Deflecting Incident Flexural Waves by Nonresonant Single-phase Meta-Slab with Subunits of Graded Thicknesses. *J Sound Vib* (2019) 454:51–62. doi:10.1016/j.jsv.2019.04.028
30. Xu Y, Fu Y, Chen H. Steering Light by a Sub-wavelength Metallic Grating from Transformation Optics. *Sci Rep* (2015) 5(1):12219. doi:10.1038/srep12219

Conflict of Interest: The authors declare that the research was conducted in the absence of any commercial or financial relationships that could be construed as a potential conflict of interest.